Control of Attosecond Entanglement and Coherence

Marc J. J. Vrakking*
Max-Born-Institut, Max-Born-Straβe 2A, 12489 Berlin, Germany

(Received 18 November 2020; accepted 5 February 2021; published 17 March 2021)

Calculations are presented of vibrational wave packet dynamics in H_2^+ ions formed by ionization of neutral H_2 by a pair of attosecond extreme ultraviolet laser pulses, using time-delayed dissociation of the cation by an ultraviolet probe pulse. The strength of experimentally observable two-level quantum beats as a function of the attosecond two-pulse delay can be related to ion + photoelectron entanglement resulting from the ionization process. This conclusion is supported by an evaluation of the purity of the reduced ion and photoelectron density matrices.

DOI: 10.1103/PhysRevLett.126.113203

The use of attosecond laser pulses generated by high-harmonic generation (HHG) has created unique opportunities for studying electron dynamics and the coupling of electronic and nuclear dynamics in a wide variety of atomic, molecular, and condensed phase systems [1–3]. Gas phase HHG is commonly understood within a three-step picture [4,5], where strong field ionization of an atomic or molecular gas is followed by photoelectron acceleration in the oscillatory laser field, and the formation of attosecond pulses occurs in an electron-ion recollision and recombination process. HHG produces attosecond pulses at extreme ultraviolet (XUV) to soft x-ray wavelengths, with photon energies that are high enough to release valence electrons from all possible atomic and molecular species.

Atomic or molecular photoionization produces a composite quantum system consisting of an ion and a photoelectron. Within a pump-probe experiment, one often only probes the pump-induced dynamics in the ion or the photoelectron. Selected examples of the former are the probing of electron localization in dissociating hydrogen molecular ions [6], the probing of valence electron dynamics in ions produced by strong field ionization using attosecond transient absorption spectroscopy [7], and the probing of charge migration in small biomolecules following their ionization by attosecond pulses [8]. Selected examples of the latter are measurements used to characterize the temporal structure of attosecond pulse trains [9] and isolated attosecond pulses [10], and Wigner time delays that occur in the course of atomic or molecular photoionization [11,12]. All these measurements rely on coherence, i.e., well-defined phase relationships between different parts of the ionic, respectively electronic wave function, which interfere in a final state of the system that is connected to the delay-dependent observable being measured.

However, composite ion + photoelectron quantum systems may be subject to significant quantum mechanical entanglement [13–16]. This entanglement limits the coherence that the observation of delay-dependent observables related to the ion or the photoelectron relies on [17]. Here, calculations will be presented where a pair of attosecond pulses (with a variable time delay) is used to ionize H_2, producing a vibrational wave packet in the H_2^+ cation [18]. The coherence properties of the vibrational wave packet are constrained by the entanglement between the molecular ion and the photoelectron, and can be controlled by the attosecond two-pulse delay. This control is revealed in two ways, namely (1) by relating the spectral characteristics of the attosecond pulse pair to the Fourier transform power spectrum (FTPS) of experimentally accessible, pump-probe delay-dependent fragment ion kinetic energy distributions resulting from a two-color XUV + UV (ultraviolet) pump-probe sequence, and (2) by calculating the purity from the reduced ion density matrix and the reduced photoelectron density matrix. By tuning the time delay between the pair of attosecond pulses, one alternates between situations where the degree of ion + photoelectron entanglement is low, and where—accordingly—the degree of vibrational coherence in the H_2^+ is high, and situations where the entanglement is high and the degree of vibrational coherence low.

The use of pairs of laser pulses within pump-probe sequences has a long history and underlies both multidimensional time-domain spectroscopy [19] and time-domain Fourier transform spectroscopy [20,21]. Its use in the XUV domain has already been demonstrated [22]. When considered in the frequency domain, a pair of identical laser pulses with a relative delay τ displays spectral fringes with a spacing $\Delta\omega = 2\pi/\tau$. The spectral intensity at a selected frequency ω undergoes one full oscillation when scanning the time delay between 0 and $\tau = 2\pi/\omega$. Therefore, τ can control the population of excited states, permitting the determination of resonance positions with exquisite spectral resolution [23], and allowing the observation of intricate quantum carpets in experiments with wavelength-tunable probe pulses [24].

Here, a pair of XUV pulses is used to prepare a vibrational wave packet in the $1s\sigma_g$ ground electronic state of H_2^+. Given that an XUV photon energy is used that exceeds the ionization potential of H_2 by about 5 eV, the population of individual vibrational states $H_2^+(v)$ does not depend on τ. However, τ influences the photoelectron spectrum accompanying each vibrational state, and hence controls the entanglement between the cation and its accompanying photoelectron. This entanglement determines the vibrational coherence that can be observed within a calculated XUV + UV pump-probe sequence.

The calculations were performed by propagating the time-dependent Schrödinger equation (TDSE) on a two-dimensional (2D) grid assuming a hydrogen molecule aligned along the polarization axis of the XUV pump and UV probe lasers, with one grid dimension reserved for the internuclear motion and one for the motion of the electron to be ionized. The remaining electron was assumed to stay bound. In line with these assumptions, the Hamiltonian is written as [25]

$$H(x,R,t) = T_e(x) + T_N(R) + V_{eN}(x,R) + V_N(R) + V_{\text{laser}}(t)\,, \quad (1)$$

with x and R the electronic and internuclear coordinate, $T_e(x)$ and $T_N(R)$ the electronic and nuclear kinetic energy, $V_{eN}(x,R)$ the soft-core Coulomb interaction of the electron with the H_2^+ cation, $V_N(R)$ the $1s\sigma_g$ or $2p\sigma_u$ H_2^+ potential energy, and $V_{\text{laser}}(t)$ the two-color laser electric field. In order to solve the TDSE, the wave function was written as

$$\Psi(x,R,t) = \Psi_g(x,R,t)\phi_g(R) + \Psi_u(x,R,t)\phi_u(R), \quad (2)$$

where $\Psi_g(x,R,t)$ and $\Psi_u(x,R,t)$ describe the 2D electron-nuclear motion, and $\phi_g(R)$ and $\phi_u(R)$ are wave functions of the bound electron, whose explicit form is not needed. The $1s\sigma_g$ and $2p\sigma_u$ potential energy curves $V_N(R)$ were taken from [26] and dipole coupling matrix elements between the $1s\sigma_g$ and the $2p\sigma_u$ states were approximated as $\langle\phi_u|\vec{e}.\vec{x}|\phi_g\rangle = \langle\phi_g|\vec{e}.\vec{x}|\phi_u\rangle \approx R/2$. The TDSE was solved using the Crank-Nicolson method on a 2D grid restricted to $R \leq 12.8$ a.u. ($\delta R = 0.025$ a.u.) and $|x| \leq 3276.8$ a.u. ($\delta x = 0.4$ a.u.), with absorbing boundaries at $R = 10$ a.u. and $|x| = 3000$ a.u. The photoelectron resulting from ionization by the XUV pulse pair reaches the absorbing boundary well within the range of times that are of interest for monitoring the vibrational dynamics in the H_2^+ cation. Therefore, the time-dependent surface flux (TSURFF) method [27] was implemented to calculate the joint energy spectrum (JES) [25,28], i.e., the differential probability for a kinetic energy release $E_k = k^2/2\mu_N$ in the UV-induced dissociation of H_2^+ (with μ_N the cationic reduced mass) in combination with a photoelectron energy $E_e = p^2/2\mu$ (with μ the mass of the electron). Within TSURFF, a boundary is defined beyond which $V_{eN}(x,R)$ can be ignored, and the wave function flux that moves beyond this boundary provides a source term within a 1D calculation of the H_2^+ vibrational dynamics [25]. The boundary where the flux was evaluated was placed at $|x_s| = 200$ a.u. The use of a substantially larger grid, as described above, was motivated by the calculations presented in Fig. 4. The TSURFF method was also applied to determine the H^+ fragment ion kinetic energy release. This implied the definition of a boundary (at $R = 8$ a.u.) beyond which $V_N(R)$ can be ignored. cos-squared laser pulses were used with the laser electric fields given by

$$E_{\text{XUV}}(t) = E_0 \left\{ \begin{array}{c} \cos^2[\alpha_{\text{XUV}} t]\cos[\omega_{\text{XUV}} t] \\ +\cos^2[\alpha_{\text{XUV}}(t-\tau)]\cos[\omega_{\text{XUV}}(t-\tau)] \end{array} \right\}, \quad (3)$$

with $\alpha_{\text{XUV}} = \omega_{\text{XUV}}/2N_{\text{XUV}}$, with N_{XUV} the number of XUV cycles, and analogously

$$E_{\text{UV}}(t) = E_1 \cos^2[\alpha_{\text{UV}}(t - t_{\text{UV}})]\cos[\omega_{\text{UV}}(t - t_{\text{UV}})]\,. \quad (4)$$

In these expressions, $t = 0$ and $t = \tau$ correspond to the maxima of the two attosecond XUV pulses and $t = t_{\text{UV}}$ corresponds to the maximum of the UV probe pulse. Figure 1 shows a sample calculation, where H_2 was ionized by a pair of $\omega_{\text{XUV}} = 0.8$ a.u. (21.76 eV), ten-cycle ($\Delta t_{\text{FWHM}} = 690$ as) pulses with a relative delay $\tau = 500$ a.u. (12.1 fs) and with $E_0 = 0.001$ a.u., and where the H_2^+ vibrational wave packet was dissociated at a variable delay by a $\omega_{\text{UV}} = 0.114$ a.u. (3.1 eV, corresponding to a

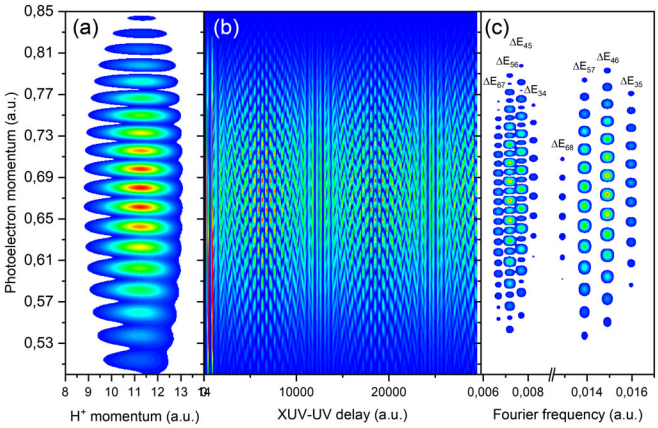

FIG. 1. (a) Joint energy spectrum (JES) for a pump-probe experiment where H_2 is ionized by a pair of ten-cycle, $\omega_{\text{XUV}} = 0.8$ a.u. (21.76 eV) laser pulses with a relative delay of 500 a.u. (12.1 fs) and dissociated at an XUV-UV delay of 10 000 a.u. (242 fs) by a five-cycle, $\omega_{\text{UV}} = 0.114$ a.u. (3.1 eV) probe laser pulse; (b) JES at $k = 11$ a.u., as a function of the XUV-UV delay; (c) Fourier transform power spectrum (FTPS) obtained from (b), revealing that the measurements can be described in terms of a number of nearest-neighbor and next-nearest-neighbor quantum beats.

wavelength of 400 nm), five-cycle ($\Delta t_{\mathrm{FWHM}} = 2.4$ fs) probe pulse with $E_1 = 0.004$ a.u. The JES for a pump-probe delay of $t_{\mathrm{UV}} = 10\,000$ a.u. (242 fs) is shown in Fig. 1(a). This figure reveals that the photoelectron momentum distribution is modulated with a period $\Delta p \approx 0.018$ a.u., corresponding to an energy spacing $\Delta E_e = p\Delta p \approx 0.0124$ a.u., in agreement with the spectral fringes in the XUV spectrum $\Delta\omega = 2\pi/\tau$. Reflecting one-photon dissociation of the cationic vibrational wave packet, the JES smoothly varies as a function of the proton momentum k. Figure 1(b) shows the calculated fragment ion yield (for $k = 11$ a.u., i.e., at the center of the JES) as a function of the photoelectron momentum and the XUV + UV pump-probe delay. For each chosen photoelectron momentum, the delay-dependent fragment ion yield shows the dephasing and rephasing that is expected for a vibrational wave packet [29], with the first revival occurring after about 12 000 a.u. (290 fs), in agreement with the experiments in [18]. However, the figure also shows that the delay-dependent fragment ion yield depends on the momentum of the accompanying photoelectron, i.e., the observation of the vibrational wave packet dynamics is entangled with the properties of the accompanying photoelectron.

This entanglement is more clearly revealed in Fig. 1(c), which shows the FTPS of the calculation shown in Fig. 1(b). At each photoelectron momentum, the delay-dependent fragment ion yield (evaluated at $k = 11$ a.u.) is described by a number of beat frequencies $\Delta E_{v_i v_j}$, arising from the coherent preparation of a superposition of H_2^+ vibrational states in the XUV ionization process. As indicated, these beat frequencies can readily be assigned to pairs of vibrational states of the H_2^+ cation, and correspond predominantly to nearest-neighbor and next-nearest-neighbor coherences. Clearly, the observed beat frequencies depend on the photoelectron momentum for which the observation is made. However, in most experiments (see, e.g., [11,18]), these photoelectrons are never measured, and one is primarily interested in observation of the cationic wave packet dynamics. Therefore, it is relevant to consider how the strength of these beat frequencies in the FTPS depends on the properties of the pump pulse. This is done in Fig. 2, which shows the intensities of the peaks in the FTPS integrated over photoelectron momentum p, as a function of the delay τ between the pair of XUV pulses. The observability of all the nearest-neighbor [Fig. 2(a)] and next-nearest-neighbor coherences [Fig. 2(b)] is related to τ in a simple manner: for a coherence involving vibrational states v_i and v_j the intensity of the corresponding peak in the FTPS is maximal if $\tau^* \Delta E_{v_i v_j} = 2n\pi$, with n an integer, and is minimal if $\tau^* \Delta E_{v_i v_j} = (2n+1)\pi$. As we will demonstrate, this is a direct consequence of the ion + photoelectron entanglement that arises in the XUV photoionization process. Crucially, and contrasting with earlier work on Fourier transform spectroscopy using bound states (see, e.g., [20,24]), the dependence of the intensity of the peaks in the FTPS on τ is not a consequence of τ-dependent variations in the populations of the participating states v_i and v_j. In fact, except near time overlap of the two XUV pulses, these populations do not depend on τ at all.

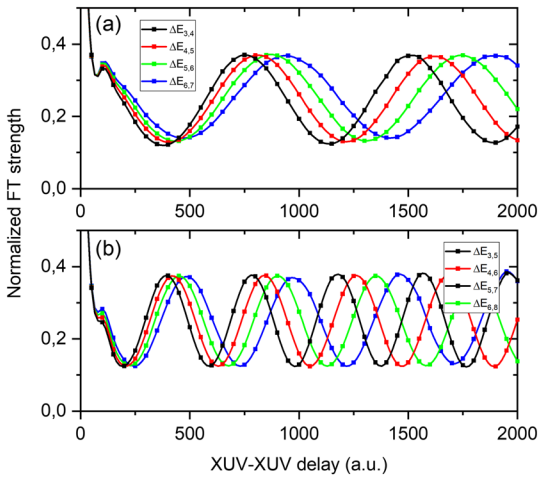

FIG. 2. (a) Intensity of nearest-neighbor quantum beats (a) and next-nearest-neighbor quantum beats (b) in the Fourier transform power spectrum (FTPS) (see Fig. 1) as a function of the XUV two-pulse delay. The peak intensities oscillate with a period that is inversely proportional to the level spacing between the two involved vibrational levels.

The way that entanglement underlies the results shown in Figs. 1 and 2 is explained in Fig. 3. This figure shows the photoelectron spectra that accompany ionization resulting

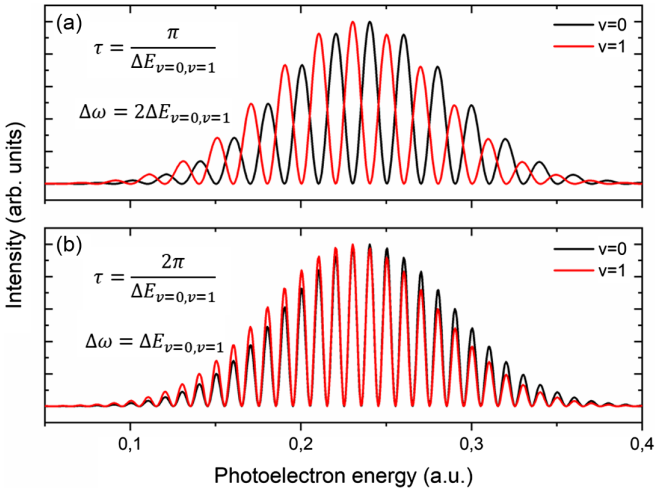

FIG. 3. The influence of the XUV two-pulse time delay τ on photoelectron spectra accompanying the formation of $H_2^+(v=0)$ and $H_2^+(v=1)$ in ionization by a ten-cycle, $\omega = 0.8$ a.u. laser field. In the picture at the top (a), a measurement of the photoelectron kinetic energy provides a strong indication whether $H_2^+(v=0)$ or $H_2^+(v=1)$ has been formed, i.e., ion + photoelectron entanglement limits the observable vibrational coherence. By contrast, in the picture at the bottom (b), a measurement of the photoelectron kinetic energy provides hardly any information on whether $H_2^+(v=0)$ or $H_2^+(v=1)$ has been formed.

in final states $H_2^+(v_i = 0)$ and $H_2^+(v_j = 1)$ for two values of the XUV pulse pair delay τ, namely $\tau = (\pi/\Delta E_{v_i v_j})$ (top) and $\tau = (2\pi/\Delta E_{v_i v_j})$ (bottom). In the former case, the XUV spectrum is modulated with a fringe spacing that equals $\Delta\omega = 2\Delta E_{v_i v_j}$. As a result the fringe patterns in the photoelectron spectra accompanying the formation of $H_2^+(v_i)$ and $H_2^+(v_j)$ are offset from each other, implying that—regardless of whether one performs this measurement or not—a possible coincident measurement of the photoelectron kinetic energy provides a strong indication for the ionic state [$H_2^+(v_i)$ or $H_2^+(v_j)$] that accompanies this photoelectron. In other words, in this case the ion and the photoelectron are strongly entangled, and the degree of coherence of the ionic wave function is very low. By contrast, in the latter case, the XUV spectrum is modulated with a fringe spacing that equals $\Delta\omega = \Delta E_{v_i v_j}$, and the photoelectron spectra accompanying the formation of $H_2^+(v_i)$ and $H_2^+(v_j)$ significantly overlap, so that a possible coincident measurement of the photoelectron kinetic energy does not provide any significant clues for the identification of the accompanying ionic state [$H_2^+(v_i)$ or $H_2^+(v_j)$]. In other words, in this case the ion and the photoelectron are only very weakly entangled, and the contribution arising from the coherent preparation of $H_2^+(v_i)$ and $H_2^+(v_j)$ is prominently visible in the FTPS (Fig. 1).

In quantum information science, there exist a number of measures that allow us to quantify the degree of entanglement in a wave function that consists of a sum of products of component wave functions describing parts of the quantum system only (such as the photoelectron and the ion, in the present case) [30]. One of these is the purity of the reduced density matrices of the subsystems, which can be obtained as

$$P = \mathrm{Tr}(\rho^2), \tag{5}$$

where ρ is the reduced density matrix for the ion or the photoelectron. In both cases the purity is given as

$$P = \sum_{i,i',j,j'} \psi_{ij}\psi_{i'j'}\psi^*_{i'j}\psi^*_{ij'}/\zeta^2\,, \tag{6}$$

where i, i' and j, j' refer to the discretization of the wave function along the internuclear and electronic grid dimension, and ζ is the norm of the wave function. Restricting the evaluation to $x > 400$ a.u. (corresponding to ionization of the molecule), Fig. 4 shows the purity of the reduced ion and photoelectron density matrices as a function of the delay τ between the two ionizing XUV pulses. The purity shows clear oscillations as a function of τ, which agree with the oscillations in the strength of the peaks in the FTPS shown in Fig. 2. For delays equal to an integral number of the average vibrational period that plays a role in the calculation ($\tau = mT_{\mathrm{vib}}$) the purity of the reduced density matrices is high, because the ion + photoelectron entanglement is low. By contrast, for delays that are a half-integral multiple of the average vibrational period the purity of the reduced density matrices is low, as a result of a high degree of entanglement between the ion and the photoelectron. Figure 4(a) shows calculations of the purity of the reduced density matrices for a number of XUV pulse durations. The purity, which only weakly depends on the XUV photon energy (not shown), significantly reduces with an increase of the number of cycles in the XUV pulse and a corresponding reduction of the XUV bandwidth, as a direct consequence of the increasing ability to identify the cationic vibrational state from a possible measurement of the accompanying photoelectron.

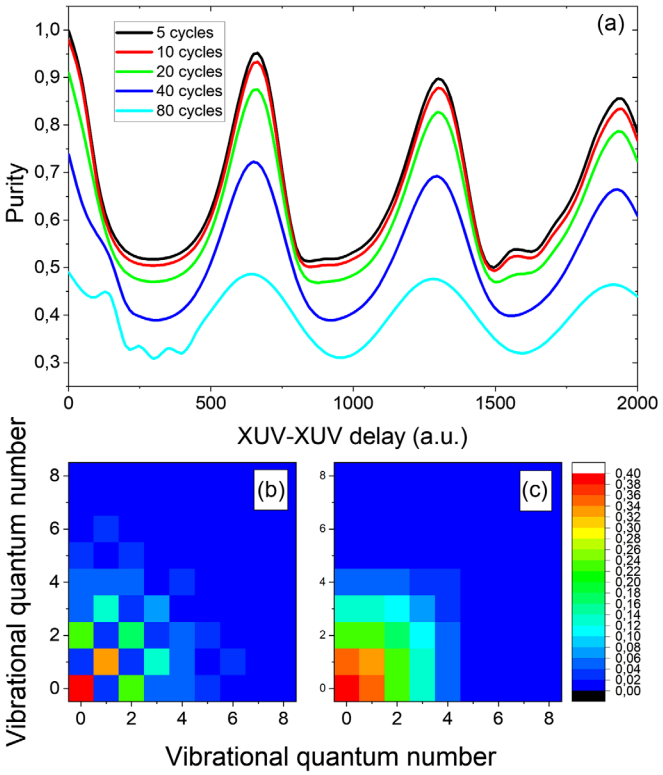

FIG. 4. (a) Calculated purity of the 2D reduced ion and photoelectron density matrices, evaluated after propagation of the TDSE over 4000 a.u. (96.7 fs), as a function of the XUV-XUV two-pulse delay. In order to isolate the contribution corresponding to XUV-induced ionization, the evaluation of the reduced density matrices was restricted to $|x| > 400$ a.u.; (b) and (c) reduced ionic density matrix, where the ionic wave function was projected onto H_2^+ vibrational states, for an XUV-XUV delay of 300 a.u. (b) and 650 a.u. (c). In both cases the diagonal elements of the reduced density matrix reproduce, indicating that the population of the vibrational states is not affected by the XUV-XUV delay. The off-diagonal elements, which characterize the vibrational coherence, are substantially different in the two cases, with the nearest-neighbor ($\Delta v = 1$) coherences almost fully suppressed in (b). This suppression is a consequence of ion + photoelectron entanglement.

Further insight into the reduced density matrices is given in Figs. 4(b) and 4(c). These figures show the reduced ionic density matrix [following projection of the H_2^+ wave function onto the vibrational eigenstates of the $H_2^+(1s\sigma_g)$ state], for $\tau = 300$ a.u. and $\tau = 650$ a.u. In agreement with the previous discussion, the high degree of ion + photoelectron entanglement for $\tau = 300$ a.u. is reflected in the absence of nearest-neighbor coherences in the reduced density matrix. By contrast, these nearest-neighbor coherences are prominently visible for $\tau = 650$ a.u.

In conclusion, we have demonstrated that the coherence in pump-probe experiments using ionizing pump laser pulses, which is a highly common situation in attosecond science, is constrained by quantum mechanical entanglement between the ion that is formed and its accompanying photoelectron. This ion + photoelectron entanglement has profound consequences for the ability to observe coherent dynamics in the ion and/or photoelectron. We have furthermore shown that the degree of ion + photoelectron entanglement can be controlled by using a pair of attosecond XUV laser pulses with a controlled interpulse delay. The ability to tailor the properties of attosecond XUV light sources to the spectroscopic properties of the system under investigation may prove advantageous in future experiments, such as, for example, experiments targeting the observation of charge migration in polyatomic and biomolecules.

*marc.vrakking@mbi-berlin.de

[1] F. Krausz and M. Ivanov, Attosecond physics, Rev. Mod. Phys. **81**, 163 (2009).

[2] S. R. Leone *et al.*, What will it take to observe processes in 'real time'?, Nat. Photonics **8**, 162 (2014).

[3] F. Calegari, G. Sansone, S. Stagira, C. Vozzi, and M. Nisoli, Advances in attosecond science, J. Phys. B **49**, 062001 (2016).

[4] K. J. Schafer, B. Yang, L. F. DiMauro, and K. C. Kulander, Above Threshold Ionization Beyond the High Harmonic Cutoff, Phys. Rev. Lett. **70**, 1599 (1993).

[5] P. B. Corkum, Plasma Perspective on Strong-Field Multiphoton Ionization, Phys. Rev. Lett. **71**, 1994 (1993).

[6] G. Sansone *et al.*, Electron localization following attosecond molecular photoionization, Nature (London) **465**, 763 (2010).

[7] E. Goulielmakis *et al.*, Real-time observation of valence electron motion, Nature (London) **466**, 739 (2010).

[8] F. Calegari *et al.*, Ultrafast electron dynamics in phenylalanine initiated by attosecond pulses, Science **346**, 336 (2014).

[9] P. M. Paul *et al.*, Observation of a train of attosecond pulses from high harmonic generation, Science **292**, 1689 (2001).

[10] R. Kienberger *et al.*, Steering attosecond electron wave packets with light, Science **297**, 1144 (2002).

[11] M. Schultze *et al.*, Delay in photoemission, Science **328**, 1658 (2010).

[12] M. Isinger *et al.*, Photoionization in the time and frequency domain, Science **358**, 893 (2017).

[13] M. Vatasescu, Entanglement between electronic and vibrational degrees of freedom in a laser-driven molecular system, Phys. Rev. A **88**, 063415 (2013).

[14] M. Ruberti, P. Decleva, and V. Averbukh, Full ab initio many-electron simulation of attosecond molecular pump–probe spectroscopy, J. Chem. Theory Comput. **14**, 4991 (2018).

[15] M. Ruberti, Onset of ionic coherence and ultrafast charge dynamics in attosecond molecular ionisation, Phys. Chem. Chem. Phys. **21**, 17584 (2019).

[16] T. Nishi, E. Lötstedt, and K. Yamanouchi, Entanglement and coherence in photoionization of H_2 by an ultrashort XUV laser pulse, Phys. Rev. A **100**, 013421 (2019).

[17] S. Carlström, J. Mauritsson, K. J. Schafer, A. L'Huillier, and M. Gisselbrecht, Quantum coherence in photo-ionisation with tailored XUV pulses, J. Phys. B **51**, 015201 (2018).

[18] F. Kelkensberg *et al.*, Molecular Dissociative Ionization and Wave-Packet Dynamics Studied Using Two-Color XUV and IR Pump-Probe Spectroscopy, Phys. Rev. Lett. **103**, 123005 (2009).

[19] M. C. Asplund, M. T. Zanni, and R. M. Hochstrasser, Two-dimensional infrared spectroscopy of peptides by phase-controlled femtosecond vibrational photon echoes, Proc. Natl. Acad. Sci. U.S.A. **97**, 8219 (2000).

[20] N. F. Scherer, R. J. Carlson, A. Matro, M. Du, A. J. Ruggiero, V. Romero-Rochin, J. A. Cina, G. R. Fleming, and S. A. Rice, Fluorescence-detected wave packet interferometry: Time resolved molecular spectroscopy with sequences of femtosecond phase-locked pulses, J. Chem. Phys. **95**, 1487 (1991).

[21] K. Hashimoto and T. Ideguchi, Phase-controlled Fourier-transform spectroscopy, Nat. Commun. **9**, 4448 (2018).

[22] G. S. M. Jansen, D. Rudolf, L. Freisem, K. S. E. Eikema, and S. Witte, Spatially resolved Fourier transform spectroscopy in the extreme ultraviolet, Optica **3**, 1122 (2016).

[23] D. Z. Kandula, C. Gohle, T. J. Pinkert, W. Ubachs, and K. S. E. Eikema, Extreme Ultraviolet Frequency Comb Metrology, Phys. Rev. Lett. **105**, 063001 (2010).

[24] H. Katsuki, H. Chiba, C. Meier, B. Girard, and K. Ohmori, Actively Tailored Spatiotemporal Images of Quantum Interference on the Picometer and Femtosecond Scales, Phys. Rev. Lett. **102**, 103602 (2009).

[25] L. Yue and L. B. Madsen, Dissociation and dissociative ionization of H_2^+ using the time-dependent surface flux method, Phys. Rev. A **88**, 063420 (2013).

[26] H. Olivares-Pilón and A. V. Turbiner, H_2^+, HeH and H_2: Approximating potential curves, calculating rovibrational states, Ann. Phys. (Amsterdam) **393**, 335 (2018).

[27] L. Tao and A. Scrinzi, Photo-electron momentum spectra from minimal volumes: The time-dependent surface flux method, New J. Phys. **14**, 013021 (2012).

[28] V. Mosert and D. Bauer, Dissociative ionization of H_2^+: Few-cycle effect in the joint electron-ion energy spectrum, Phys. Rev. A **92**, 043414 (2015).

[29] M. Gruebele and A. H. Zewail, Femtosecond wave packet spectroscopy: Coherences, the potential, and structural determination, J. Chem. Phys. **98**, 883 (1993).

[30] M. A. Nielsen and I. L. Chuang, *Quantum Computation and Quantum Information: 10th Anniversary Edition* (Cambridge University Press, Cambridge, England, 2010).